Selected for a Viewpoint in *Physics*

RAPID COMMUNICATIONS

PHYSICAL REVIEW B **96**, 041201(R) (2017)

Nontrivial Berry phase and type-II Dirac transport in the layered material $PdTe_2$

Fucong Fei,[1] Xiangyan Bo,[1] Rui Wang,[1] Bin Wu,[1] Juan Jiang,[2] Dongzhi Fu,[1] Ming Gao,[3] Hao Zheng,[4] Yulin Chen,[2,5] Xuefeng Wang,[3] Haijun Bu,[1] Fengqi Song,[1,*] Xiangang Wan,[1,†] Baigeng Wang,[1,‡] and Guanghou Wang[1]

[1]*National Laboratory of Solid State Microstructures, Collaborative Innovation Center of Advanced Microstructures, College of Physics, Nanjing University, Nanjing 210093, People's Republic of China*

[2]*School of Physical Science and Technology, CAS-Shanghai Science Research Center, ShanghaiTech University, Shanghai 200031, People's Republic of China*

[3]*National Laboratory of Solid State Microstructures, Collaborative Innovation Center of Advanced Microstructures, School of Electronic Science and Engineering, Nanjing University, Nanjing 210093, People's Republic of China*

[4]*Department of Physics and Astronomy, Shanghai Jiao Tong University, Shanghai 200240, People's Republic of China*

[5]*Department of Physics, University of Oxford, Oxford OX1 3PU, United Kingdom*

(Received 26 January 2017; revised manuscript received 28 April 2017; published 5 July 2017)

We report on a systematic study of type-II Dirac fermions in a layered crystal of $PdTe_2$. De Haas–van Alphen oscillations show a small Fermi-surface pocket with a cross section of 0.077 nm^{-2} with a nontrivial Berry phase. First-principles calculation reveals that the nontrivial Berry phase originates from a hole pocket formed by the tilted Dirac cone. In addition, the band dispersion measured with angle-resolved photoemission spectroscopy is found to be consistent with that of a type-II Dirac cone dispersion. We propose that $PdTe_2$ is an improved platform to host topological superconductors.

DOI: 10.1103/PhysRevB.96.041201

Introduction. In condensed matter, multiple excitations can be implemented to simulate the physics of new particles, such as Dirac fermions [1–10], Weyl fermions [11–24], Majorana fermions [25–28], and exotic new fermions beyond Dirac and Weyl fermions [29] with the potential applications in next-generation spintronics and quantum computing. These particles might be unrealistic in the real world whereas allowable in condensed matter due to versatile operations of symmetry breaking. In Dirac semimetals, e.g., Na_3Bi [8–10] and Cd_3As_2 [1–7], topological insulators [30–33] and topological protected gapless Dirac cones with liner dispersions are discovered, and electrons in these materials can be described by a massless Dirac equation. By breaking inversion symmetry or time-reversal symmetry, a Dirac cone can split into a pair of Weyl cones and form Weyl semimetals, such as the TaAs family [12–17]. Noncontinuous Fermi arcs appear on their surfaces, and interesting negative magnetoresistance appears, which simulates the chiral anomaly in high-energy physics. In several Weyl semimetals, for instance, $Mo_xW_{1-x}Te_2$ [19–23] and LaAlGe [11], the Lorentz invariance is broken, and the Weyl cones are tilted strongly to form type-II Weyl semimetals, which are predicted to have unique properties, such as field-selective anomaly and chiral mode reversal [34], as well as Klein tunneling in momentum space [35]. Recently, the Lorentz invariance breaking is suggested in Dirac semimetals with the result of type-II Dirac fermions with a tilted Dirac cone in the $PtSe_2$ family [36–38].

Here we report the Shubnikov–de Haas (SdH) and de Haas–van Alphen (dHvA) oscillations in a layered material $PdTe_2$, and a nontrivial Berry phase is demonstrated here. Six conductive pockets are identified in the dHvA measurements where the α mode with a frequency of 8.0 T exhibits the nontrivial Berry phase. The calculations confirm the Berry phase is originated from the hole pocket of a tilted type-II Dirac cone. This also is confirmed by the dispersions in angle-resolved photoemission spectroscopy (ARPES). Remembering its anisotropic superconductivity (SC) under 1.9 K, we suggest $PdTe_2$ might be an improved platform to host the topological superconductors (TSCs).

Experiment. Single-crystal $PdTe_2$ was grown by the melt-growth method. A certain amount of Pd and Te powder (from Alfa Aesar) with an atomic ratio of 1:2.2 was sealed in an evacuated ampoule. The ampoule was heated up and maintained at 790 °C for 48 h. The melt then was cooled down slowly to 500 °C for 7 days and then annealed at this temperature for seven more days before natural cooling to room temperature. Millimeter-sized crystals with metallic luster were obtained, which easily could be exfoliated to small flakes by a knife. As shown in Fig. 1(a), $PdTe_2$ is a type of layered transition-metal dichalcogenide material of a CdI_2-type structure with the $P\bar{3}m1$ space group. The x-ray-diffraction data of the single crystal is shown in Fig. 1(b). The strong $(00n)$ peaks of $PdTe_2$ can clearly be seen, and no other impurity peaks can be found, indicating nice crystallization of the $PdTe_2$ sample. Figure 1(c) shows the energy-dispersive spectra (EDS) for a typical $PdTe_2$ flake. The ratio between Pd and Te elements is 1:1.99, indicating the stoichiometric ratio of the sample. The EDS mapping [insets of Fig. 1(c)] show the uniform elemental distribution of Pd and Te, respectively. Figure 1(d) is the Raman spectrum and shows two peaks at 74.1 and 131.5 cm^{-1}, respectively.

Results and discussion. (A) Electrical transport properties. We measure the magnetoresistance of a $PdTe_2$ single crystal up to 33.5 T under 1.7 K. The longitudinal resistance is shown in Fig. 2(a), and SdH oscillations can be identified above 15 T as seen in the inset, indicating the high quality of the crystal. Figure 2(b) shows the Hall resistance under various temperatures from 2 to 150 K. One can clearly see the Hall resistance versus the magnetic field is linear at

*Corresponding author: songfengqi@nju.edu.cn
†Corresponding author: xgwan@nju.edu.cn
‡Corresponding author: bgwang@nju.edu.cn

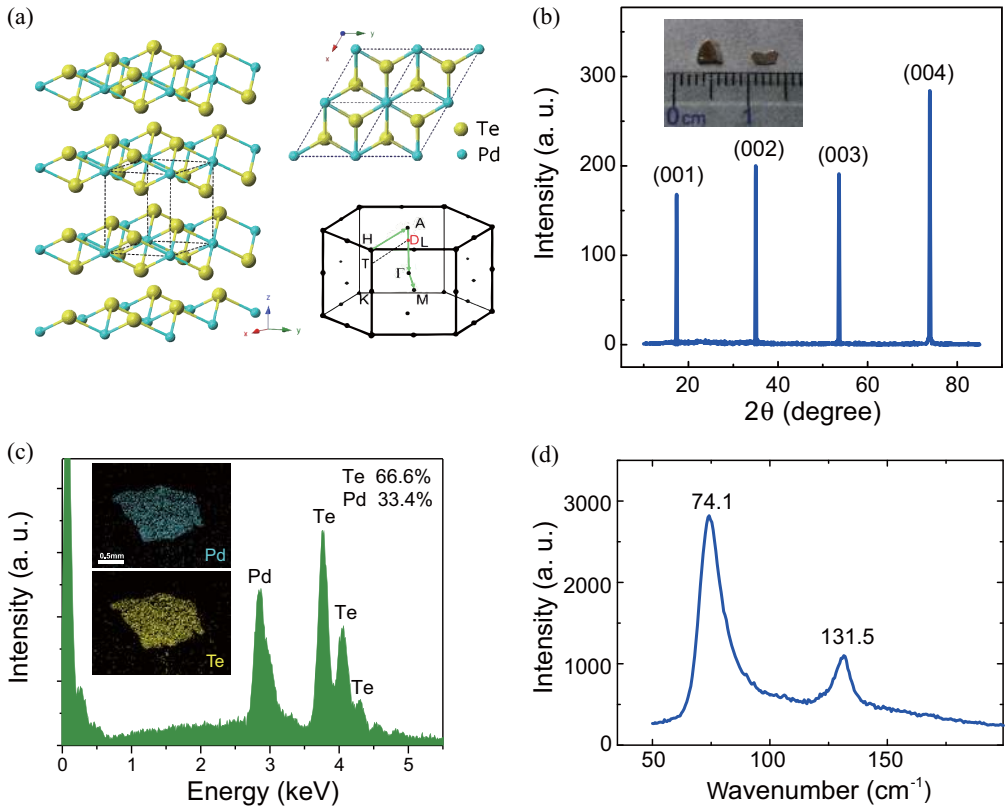

FIG. 1. $PdTe_2$ crystal growth and characterization. (a) The CdI_2-type crystal structure of $PdTe_2$ and the corresponding Brillouin zone (lower right panel) (b) The x-ray-diffraction data of the $PdTe_2$ sample. Strong $(00n)$ peaks can be seen. The inset is the optical micrograph of several flakes. (c) The EDS spectrum indicates the stoichiometric ratio of the sample. The insets show the EDS mapping of Pd and Te, respectively, of a typical flake. (d) Raman spectrum of the $PdTe_2$ crystal.

150 K but becomes bent when the temperature goes down to 2 K, indicating the multiple band transport with complex contributions from various conductive pockets near the Fermi surface [39].

$PdTe_2$ is a superconductor with $T_c \sim 2$ K [40]. We perform a further study on the superconductivity property of $PdTe_2$. The crystal shows an anisotropic superconductivity as seen when we measure the temperature-dependent resistance under a magnetic field using two different sets of devices for configurations 1 (the current is perpendicular to the c axis; the field is parallel to the c axis) and 2 (the current is parallel to the c axis; the field is parallel to the c axis) as seen in Figs. 2(c) and 2(d), respectively. Using configuration 2, with increasing the field to 500 Oe, the superconductivity nearly is suppressed whereas the superconductivity survives the field of 2000 Oe in configuration 1. We can also see that, in Fig. 2(d), the resistance increases when temperature goes down near T_c, which is absent in Fig. 2(c). The anisotropic superconductivity in $PdTe_2$ is thus obvious.

(B) dHvA oscillations and the nontrivial Berry phase. The nontrivial Berry phase is demonstrated by the dHvA measurements after we measure the magnetization condition of the $PdTe_2$ flakes under low temperatures. Figure 3(a) displays the magnetization versus the magnetic field ($B \parallel c$) for $PdTe_2$ at 1.8 K. Beautiful dHvA oscillations can be seen from the raw data of the M-H curves. Figure 3(b) shows the magnetization strength versus $1/B$ under various temperatures after the background subtraction. Multiple sets of oscillations with the frequencies of 8.0 (α), 113.2 (β), 117.9 (γ), 124.3 (δ), 133.9 (ε), and 455.8 T (ζ) can be extracted from the M-H data by the fast Fourier transformation (FFT) [the inset in Fig. 3(c)]. The dHvA oscillation can be described by the Lifshitz-Kosevich (LK) formula [41],

$$\Delta M \propto -R_T R_D \sin\left\{2\pi\left[\frac{F}{B} - \left(\frac{1}{2} - \phi\right)\right]\right\}. \quad (1)$$

The thermal damping factor is $R_T = \frac{\chi T}{\sinh(\chi T)}$, and the Dingle damping factor is $R_D = \exp(-\chi\, T_D)$ where $\chi = \frac{2\pi^2 k_B m^*}{\hbar e B}$. ϕ is the phase shift, and $\phi = \frac{\phi_B}{2\pi} - \delta$, where ϕ_B is the Berry phase and δ equals 0 and $\pm 1/8$ for two-dimensional and three-dimensional systems, respectively. The effective mass m^* can be extracted by the fit of the temperature dependence of the corresponding oscillation amplitude to R_T. The Dingle temperature T_D can also be obtained through the fit of Dingle damping factor R_D, meanwhile, quantum relaxation time τ can be calculated by $\tau = \frac{\hbar}{2\pi k_B T_D}$ and quantum mobility $\mu_q = e\tau/m^*$. The Berry phases determine the topological properties of the conductive pockets and can be extracted using the Landau-level fan diagram. In dHvA oscillation, the integer Landau index should be assigned when density of states of the Fermi surface, which is proportional to dM/dB, reaches a minimum. Therefore, the Landau index of the dHvA oscillation minima should be $n - 1/4$ [42]. We find the α

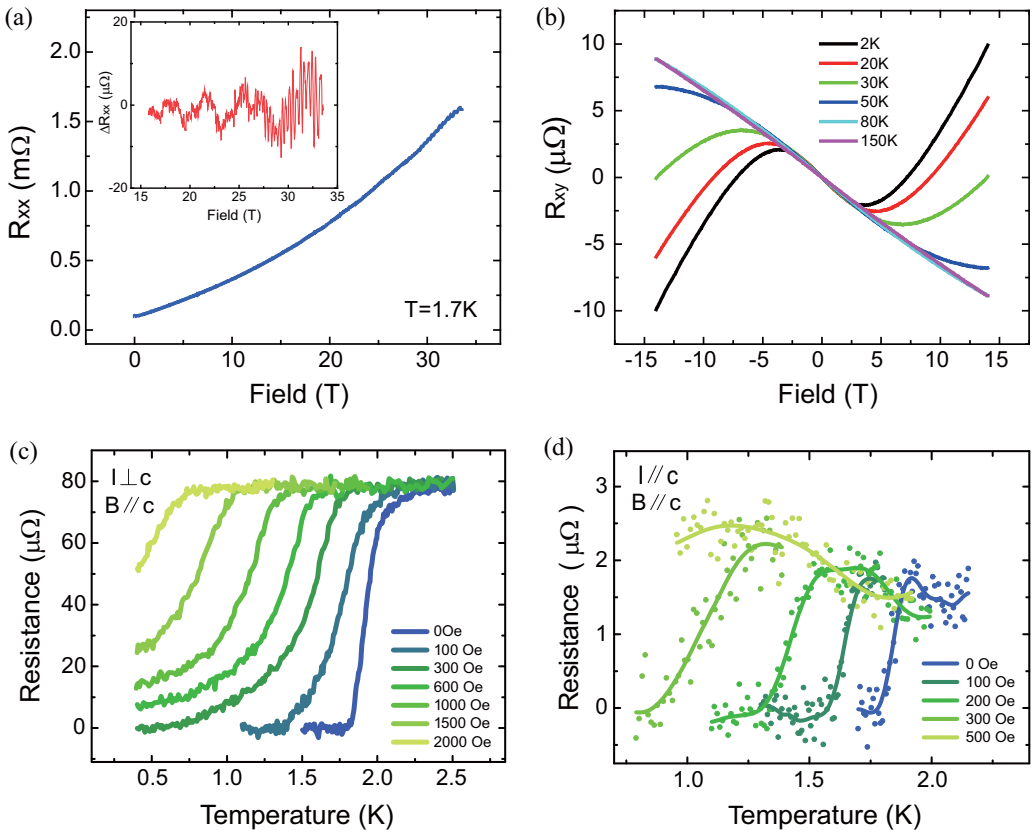

FIG. 2. Electrical transport under magnetic fields and low temperatures. (a) The magnetoresistance of $PdTe_2$ under 1.7 K. The inset shows SdH oscillation after background subtraction. (b) Hall resistance versus magnetic field under various temperatures. (c) and (d) are temperature dependence of resistance under different fields of configurations 1 ($I \perp c$, $B \parallel c$) and 2 ($I \parallel c$, $B \parallel c$), respectively, indicating anisotropic superconductivity in $PdTe_2$.

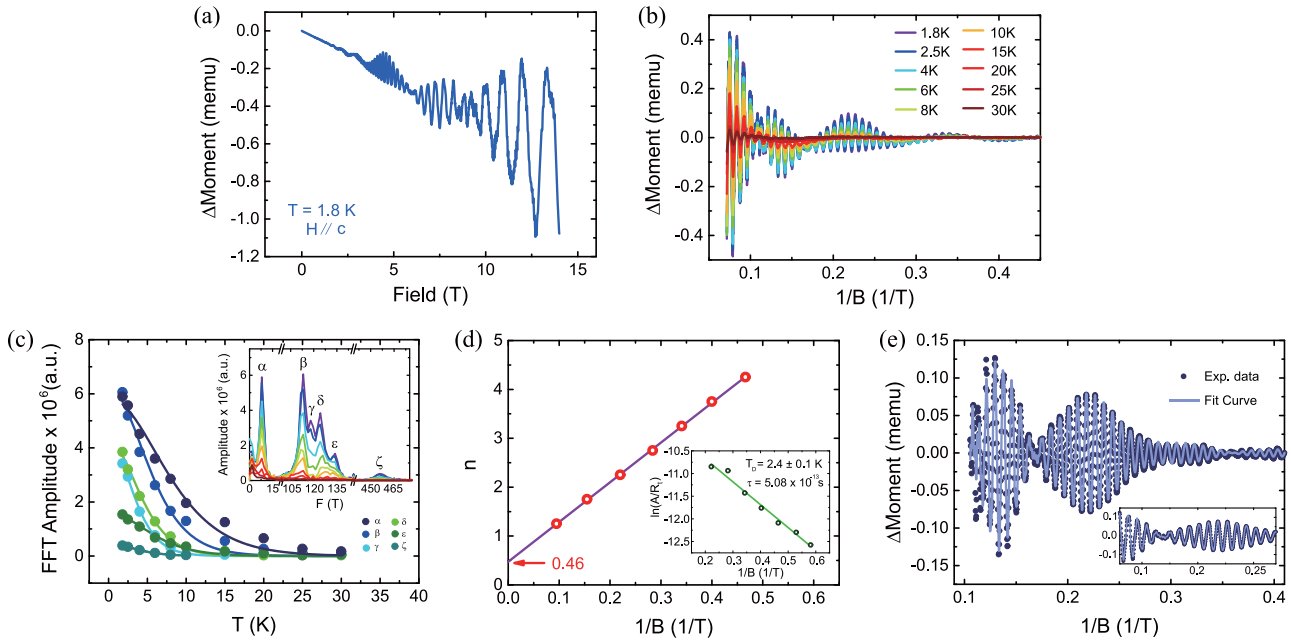

FIG. 3. The dHvA oscillations and nontrivial Berry phase. (a) The magnetization curve ($B \parallel c$) for $PdTe_2$ at 1.8 K. Beautiful dHvA oscillations can be seen. (b) The magnetization strength versus $1/B$ under various temperatures after background subtraction. (c) The fits of effective mass for all six oscillation modes (α to ζ). The inset is the FFT amplitudes versus temperature. The peaks corresponding to each oscillation mode are marked with greek letters. (d) The Landau fan diagram for the dHvA oscillation of low-frequency mode α. The inset is the fit of Dingle temperature (T_D). (e) Oscillatory component of other frequencies (β to ζ) and the multiband LK fit of it. The inset shows a part of the curve, indicating the perfect fit of the experimental data.

TABLE I. Parameters extracted from the dHvA oscillations ($H \parallel c$) of $PdTe_2$. F: oscillation frequency; S_f: cross section of the Fermi surface; k_f: the Fermi wave vector; T_D: the Dingle temperature; m^*/m_0: relative effective mass; τ: quantum relaxation time; and μ_q: quantum mobility.

F (T)	S_f (Å^{-2})	k_f (Å^{-1})	T_D (K)	m^*/m_0	τ (ps)	μ_q (cm^2 V^{-1} s^{-1})
8.0	7.67×10^{-4}	1.56×10^{-2}	2.4	0.14	0.51	6209
113.2	1.09×10^{-2}	5.88×10^{-2}	3.4	0.21	0.36	3030
117.9	1.13×10^{-2}	6.00×10^{-2}	1.9	0.33	0.65	3464
124.3	1.19×10^{-2}	6.16×10^{-2}	3.0	0.26	0.41	2722
133.9	1.28×10^{-2}	6.39×10^{-2}	6.8	0.20	0.18	1593
455.8	4.34×10^{-2}	0.118	5.7	0.29	0.21	1293

mode can be separated easily, whereas the four midfrequency modes ($\beta,\gamma,\delta,\varepsilon$) have similar frequencies. In addition, the oscillation of the high-frequency mode (ζ) is masked by other oscillations because of the small amplitude. Therefore, we fit the oscillatory components of these five modes by the multiband LK formula as shown in Fig. 3(e) and extract the transport parameters. All six sets of data of the dHvA oscillations are displayed in Table I.

Interestingly, a topological-nontrivial mode, the α mode, is evidenced by the Landau fan diagram by using the dHvA oscillation minima as the Landau index of $n - 1/4$ as shown in Fig. 3(d). The intercept of the linear fitting is 0.46, which is the signature of nontrivial Dirac transport. Figure 3(c) displays the fits of the effective mass of all the six oscillatory modes by the corresponding FFT amplitudes versus temperature [the inset in Fig. 3(c)]. It is clear that the effective mass of the low-frequency mode (α) is much less than other modes. The low effective mass also agrees with the Dirac nature of the α mode.

(C) Theoretical calculation of the band structures. To identify the contributing electronic pocket of each oscillation mode, the assistance from the band-structural calculation is needed. We calculate the band structure of $PdTe_2$ [Fig. 4(a)], and the Brillouin zone is shown in the inset of Fig. 1(a) where high-symmetry points, lines, and Dirac point (D) also are indicated. There is a band crossing feature near the Fermi level along the Γ-A line. This band crossing is unavoidable because these two bands belong to different representations (G4 and G5 + G6, respectively). This is determined by the $C3$ rotational symmetry around the c axis [36,37,43]. Remarkably, these two bands show linear dispersions in the vicinity of the Dirac point along both the in-plane (k_x-k_y) and the out-of-plane (k_z) directions, and the Dirac cone is untilted along the k_x-k_y plane [Fig. 4(d)] but tilted strongly along the (k_z) direction [Fig. 4(e)], which is the characteristic feature of the type-II Dirac fermions as reported [36,37]. By our calculations, the Dirac point is at $k = (0,0, \pm 0.40)$.

In the calculation, a series of electronic pockets can be seen on the Fermi surface as shown in Figs. 4(b) and 4(c). For figuring out the contributing pocket of each dHvA oscillation mode, we calculate the extremal surfaces of each pocket along the k_z direction. The modes around 100 T were considered contributing from the minimum extremal surfaces [yellow area in Fig. 4(b)] of six pliers-shaped pockets [translucent blue pockets in Fig. 4(b)] at $k_z = \pm 0.5$. A departure from the high-symmetry points and complex contours of these pockets may explain the several beat frequencies around 100 T. The extremal surface of the purple colored pocket at the K point in Fig. 4(b) is about 0.04 Å^{-2}, which is the possible origin of the ζ mode (456 T).

In type-II Dirac semimetals, the Dirac cone is tilted strongly because of the Lorentz invariance breaking, which causes the formation of a pair of electron and hole pockets [44]. In $PdTe_2$, the Fermi level is above the Dirac point. Thus the hole pocket shrinks to a small pocket at the Γ point as seen in Fig. 4(a) [also marked by the red dashed lines in Figs. 4(b) and 4(c)], whereas the electron pocket, which, corresponding to the translucent-aqua-like pocket in Figs. 4(b) and 4(c), becomes much bigger and forms an apple-pit-shaped pocket in reciprocal space. We find that the cut of the small hole pocket is with a similar area

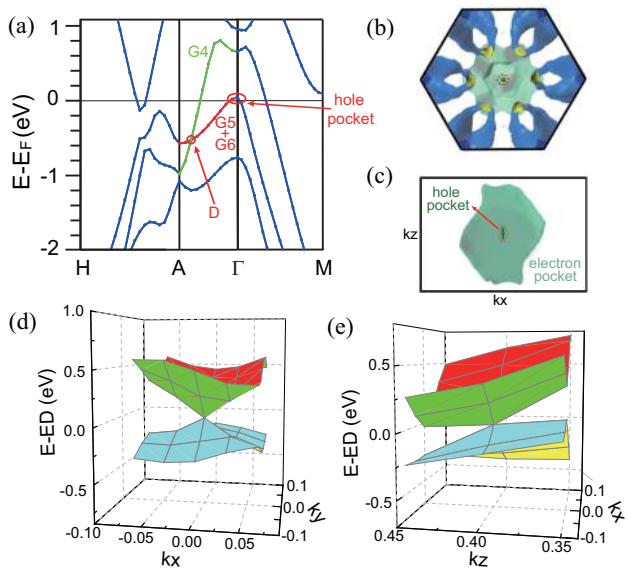

FIG. 4. Matching the dHvA components in the calculations of the type-II Dirac cone. (a) The calculated electronic structures plotted along the directions shown in the Brillouin zone [Fig. 1(a)]. The Dirac point and the small hole pocket with the α mode are marked in the panel. (b) and (c) show the contour of the Fermi surface along the k_x-k_y and k_x-k_z planes, respectively. Pockets irrelevant to the hole and electron pockets formed by the tilted Dirac cone in (c) are concealed for clearness. (d) and (e) show the projection of the Dirac cone along k_x-k_y and k_x-k_z, respectively. The Dirac cone with tilted properties along the k_z direction can clearly be seen.

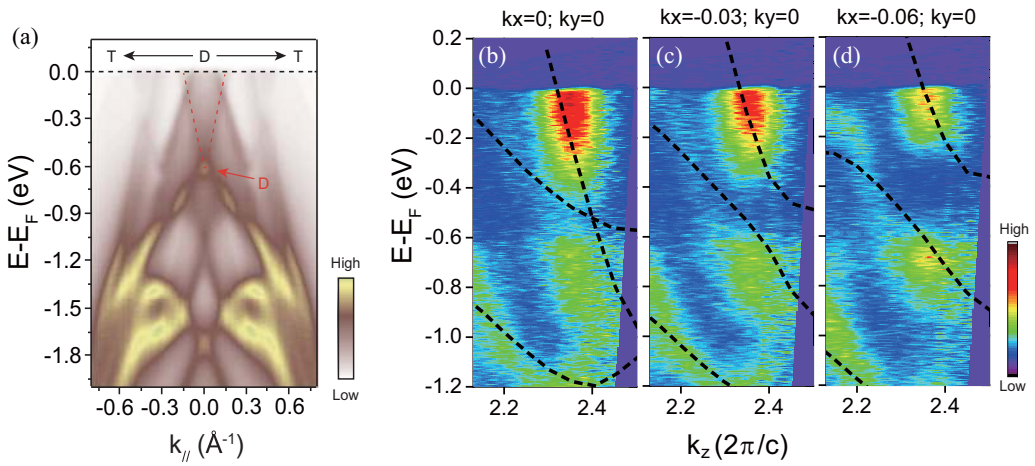

FIG. 5. ARPES measurement of $PdTe_2$. (a) The dispersion along the T-D direction measured by ARPES. The linear dispersion of the Dirac cone is labeled by the red dashed lines. The Dirac point also is marked by the red arrow. (b)–(d) are dispersions along the k_z directions. The black dashed lines are band calculations for comparison.

to that of the nontrivial α mode (8 T), which further confirms the Dirac nature of this pocket. For the big electron pocket, although the shape is complex, we verify that only a single maximum cross section is achieved when $k_z = 0$ after precise analysis. The corresponding oscillation frequency contribution is over 5 kT, which is too high to detect in our experiment.

(D) ARPES measurement of the $PdTe_2$ *samples*. The type-II Dirac dispersion in $PdTe_2$ is characterized by the ARPES measurement. Figure 5(a) shows the electronic dispersion along the T-D direction. The linear dispersion of the Dirac cone can clearly be seen. Noting that the T-D line is perpendicular to k_z, the Dirac cone is not tilted as predicted. The evolution of the Dirac cone dispersion can clearly be seen under different photon energies (see the Supplemental Material, Fig. S1 [45]), which reveals the bulk properties of the Dirac cone. According to the ARPES data under various photon energies, we map out the E-k_z dispersions as seen in Figs. 5(b)–5(d). Comparing with the calculation, ARPES dispersions are consistent with the theoretical data, and the tilted Dirac cone can be recognized when $k_x = k_y = 0$ [Fig. 5(b)]. When departing from the Γ-A line as seen from Figs. 5(b)–5(d), the two bands forming Dirac cones separate obviously in calculation as well as in our experimental data. One may notice that the intensity near the Dirac point is suppressed. This may be explained by the slight deviation from $k_x = k_y = 0$. We also map out the k_x-k_z constant energy contours when $k_y = 0$ (see the Supplemental Material, Fig. S2 [45]). A hole pocket and an electron pocket can be seen and tend to touch each other at the Dirac point when the energy goes down, which is a characteristic of type-II Dirac dispersion. The type-II property of the Dirac cone in $PdTe_2$ is thus confirmed.

(E) Discussions. We suggest the discovered type-II Dirac semimetal be an improved platform of the TSC on which a lot of effort is made [27,46–50]. Recently, with the discovery of a three-dimensional topological semimetal, the attempts are made on inducing the s-wave superconductivity in the newly discovered semimetals [51,52]. We here compare the TSC transport based on three kinds of mother materials: Weyl semimetals, Dirac semimetals, and type-II Dirac semimetals. For the TSC arisen from the Weyl semimetals, it is known from the theoretical work [51,52] that the chiral anomaly survived and invokes a Fermi arc surface state in which the electrons remain unpaired and no gap opens. Meanwhile, the effective $p_x + i\,p_y$ pairing state in the bulk leads to a chiral Majorana surface mode. The coexistence of the Fermi arc and the Majorana mode may hamper its application in quantum computation. For the TSC arisen from the Dirac semimetals, the gapless node is a Dirac point which is fourfold degenerated and additional space-group symmetries are required for the stability of the Dirac nodes. The Fermi arc state of the Dirac semimetal is not topologically stable [53]. Hence, after the superconductivity sets in, in general, the surface electrons would form Cooper pairs and gap out the surface state. The situation is improved for the case of the type-II Dirac cone where the dispersion is tilted as shown in Fig. 6. The significant superiority that can be seen is that the electron and hole pockets near the Dirac points provide the plentiful density of states which is favorable for both superconducting and TSC carrier ratios. This also means a larger carrier density in the TSC arisen from type-II Dirac semimetals.

Conclusion. To summarize, combining dHvA oscillations and the first-principles calculations, we verify the topological nontrivial Berry phase from the hole pocket of a tilted Dirac

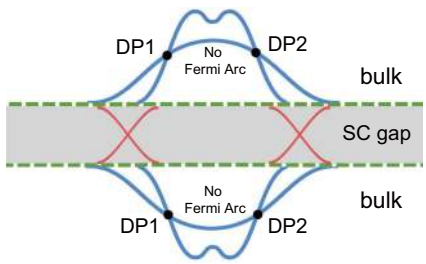

FIG. 6. Optimizing the TSC by type-II Dirac semimetals. This figure displays the band-structure diagrams of the possible topological superconductors based on the mother materials of the type-II Dirac semimetal when $T < T_c$. The red solid curves in the SC gap (gray zone) represent the Majorana chiral mode. The Fermi arc states are killed in the Dirac semimetals when the superconductivity occurs.

cone in the type-II Dirac semimetal $PdTe_2$. Angle-resolved photoemission spectroscopy also demonstrates the type-II Dirac dispersion. Anisotropic superconductivity below 1.9 K in $PdTe_2$ is confirmed by a low-temperature transport measurement. It is therefore a possible improved platform to search for mysterious Majorana fermions and to apply it to the next-generation spintronics devices.

Acknowledgments. We gratefully acknowledge financial support from the National Key Projects for Basic Research of China (Grants No. 2013CB922103 and No. 2017YFA0303200), the National Natural Science Foundation of China (Grants No. 91622115, No. 91421109, No. 61176088, No. 11522432, and No. 11274003), the Natural Science Foundation of Jiangsu Province (Grants No. BK20130054 and No. BK20160659), and the Fundamental Research Funds for the Central Universities. Use of the Stanford Synchrotron Radiation Lightsource, SLAC National Accelerator Laboratory is supported by the U.S. Department of Energy, Office of Science, Office of Basic Energy Sciences under Contract No. DE-AC02-76SF00515. Technical support from the Hefei National Synchrotron Radiation Laboratory and the High Magnetic Field Laboratory, Chinese Academy of Sciences is acknowledged. We also thank Professor Y. Tao from Nanjing Normal University, China for stimulating discussions.

F. Fei, X. Bo, and R. Wang contributed equally to this work.

[1] Z. K. Liu, J. Jiang, B. Zhou, Z. J. Wang, Y. Zhang, H. M. Weng, D. Prabhakaran, S. K. Mo, H. Peng, P. Dudin, T. Kim, M. Hoesch, Z. Fang, X. Dai, Z. X. Shen, D. L. Feng, Z. Hussain, and Y. L. Chen, Nat. Mater. **13**, 677 (2014).

[2] L. P. He, X. C. Hong, J. K. Dong, J. Pan, Z. Zhang, J. Zhang, and S. Y. Li, Phys. Rev. Lett. **113**, 246402 (2014).

[3] H. Wang, H. Wang, H. Liu, H. Lu, W. Yang, S. Jia, X. J. Liu, X. C. Xie, J. Wei, and J. Wang, Nat. Mater. **15**, 38 (2016).

[4] M. Neupane, S.-Y. Xu, R. Sankar, N. Alidoust, G. Bian, C. Liu, I. Belopolski, T.-R. Chang, H.-T. Jeng, H. Lin, A. Bansil, F. Chou, and M. Z. Hasan, Nat. Commun. **5**, 3786 (2014).

[5] S. Jeon, B. B. Zhou, A. Gyenis, B. E. Feldman, I. Kimchi, A. C. Potter, Q. D. Gibson, R. J. Cava, A. Vishwanath, and A. Yazdani, Nature Mater. **13**, 851 (2014).

[6] L. He, Y. Jia, S. Zhang, X. Hong, C. Jin, and S. Li, npj Quantum Mater. **1**, 16014 (2016).

[7] S. Borisenko, Q. Gibson, D. Evtushinsky, V. Zabolotnyy, B. Buchner, and R. J. Cava, Phys. Rev. Lett. **113**, 027603 (2014).

[8] S.-Y. Xu, C. Liu, S. K. Kushwaha, R. Sankar, J. W. Krizan, I. Belopolski, M. Neupane, G. Bian, N. Alidoust, T.-R. Chang, H.-T. Jeng, C.-Y. Huang, W.-F. Tsai, H. Lin, P. P. Shibayev, F.-C. Chou, R. J. Cava, and M. Z. Hasan, Science **347**, 294 (2015).

[9] J. Xiong, S. K. Kushwaha, T. Liang, J. W. Krizan, M. Hirschberger, W. Wang, R. J. Cava, and N. P. Ong, Science **350**, 413 (2015).

[10] Z. K. Liu, B. Zhou, Y. Zhang, Z. J. Wang, H. M. Weng, D. Prabhakaran, S.-K. Mo, Z. X. Shen, Z. Fang, X. Dai, Z. Hussain, and Y. L. Chen, Science **343**, 864 (2014).

[11] S.-Y. Xu, N. Alidoust, G. Chang, H. Lu, B. Singh, I. Belopolski, D. Sanchez, X. Zhang, G. Bian, H. Zheng, M.-A. Husanu, Y. Bian, S.-M. Huang, C.-H. Hsu, T.-R. Chang, H.-T. Jeng, A. Bansil, V. N. Strocov, H. Lin, S. Jia, and M. Z. Hasan, arXiv:1603.07318.

[12] L. X. Yang, Z. K. Liu, Y. Sun, H. Peng, H. F. Yang, T. Zhang, B. Zhou, Y. Zhang, Y. F. Guo, M. Rahn, D. Prabhakaran, Z. Hussain, S. K. Mo, C. Felser, B. Yan, and Y. L. Chen, Nat. Phys. **11**, 728 (2015).

[13] H. M. Weng, C. Fang, Z. Fang, B. A. Bernevig, and X. Dai, Phys. Rev. X **5**, 011029 (2015).

[14] N. Xu, H. M. Weng, B. Q. Lv, C. E. Matt, J. Park, F. Bisti, V. N. Strocov, D. Gawryluk, E. Pomjakushina, K. Conder, N. C. Plumb, M. Radovic, G. Autes, O. V. Yazyev, Z. Fang, X. Dai, T. Qian, J. Mesot, H. Ding, and M. Shi, Nat. Commun. **7**, 11006 (2016).

[15] B. Q. Lv, H. M. Weng, B. B. Fu, X. P. Wang, H. Miao, J. Ma, P. Richard, X. C. Huang, L. X. Zhao, G. F. Chen, Z. Fang, X. Dai, T. Qian, and H. Ding, Phys. Rev. X **5**, 031013 (2015).

[16] S.-Y. Xu, I. Belopolski, N. Alidoust, M. Neupane, G. Bian, C. Zhang, R. Sankar, G. Chang, Z. Yuan, C.-C. Lee, S.-M. Huang, H. Zheng, J. Ma, D. S. Sanchez, B. Wang, A. Bansil, F. Chou, P. P. Shibayev, H. Lin, S. Jia, and M. Z. Hasan, Science **349**, 613 (2015).

[17] H. Zheng, S.-Y. Xu, G. Bian, C. Guo, G. Chang, D. S. Sanchez, I. Belopolski, C.-C. Lee, S.-M. Huang, X. Zhang, R. Sankar, N. Alidoust, T.-R. Chang, F. Wu, T. Neupert, F. Chou, H.-T. Jeng, N. Yao, A. Bansil, S. Jia, H. Lin, and M. Z. Hasan, ACS Nano **10**, 1378 (2016).

[18] Y. Qi, P. G. Naumov, M. N. Ali, C. R. Rajamathi, W. Schnelle, O. Barkalov, M. Hanfland, S. C. Wu, C. Shekhar, Y. Sun, V. Suss, M. Schmidt, U. Schwarz, E. Pippel, P. Werner, R. Hillebrand, T. Forster, E. Kampert, S. Parkin, R. J. Cava, C. Felser, B. Yan, and S. A. Medvedev, Nat. Commun. **7**, 11038 (2016).

[19] L. Huang, T. M. McCormick, M. Ochi, Z. Y. Zhao, M. T. Suzuki, R. Arita, Y. Wu, D. X. Mou, H. B. Cao, J. Q. Yan, N. Trivedi, and A. Kaminski, Nat. Mater. **15**, 1155 (2016).

[20] X. C. Pan, X. Chen, H. Liu, Y. Feng, Z. Wei, Y. Zhou, Z. Chi, L. Pi, F. Yen, F. Song, X. Wan, Z. Yang, B. Wang, G. Wang, and Y. Zhang, Nat. Commun. **6**, 7805 (2015).

[21] Z. J. Wang, D. Gresch, A. A. Soluyanov, W. W. Xie, S. Kushwaha, X. Dai, M. Troyer, R. J. Cava, and B. A. Bernevig, Phys. Rev. Lett. **117**, 056805 (2016).

[22] I. Belopolski, S. Y. Xu, Y. Ishida, X. C. Pan, P. Yu, D. S. Sanchez, H. Zheng, M. Neupane, N. Alidoust, G. Q. Chang, T. R. Chang, Y. Wu, G. Bian, S. M. Huang, C. C. Lee, D. X. Mou, L. N. Huang, Y. Song, B. G. Wang, G. H. Wang, Y. W. Yeh, N. Yao, J. E. Rault, P. Le Fevre, F. Bertran, H. T. Jeng, T. Kondo, A. Kaminski, H. Lin, Z. Liu, F. Q. Song, S. Shin, and M. Z. Hasan, Phys. Rev. B **94**, 085127 (2016).

[23] I. Belopolski, D. S. Sanchez, Y. Ishida, X. Pan, P. Yu, S. Y. Xu, G. Chang, T. R. Chang, H. Zheng, N. Alidoust, G. Bian, M. Neupane, S. M. Huang, C. C. Lee, Y. Song, H. Bu, G. Wang,

S. Li, G. Eda, H. T. Jeng, T. Kondo, H. Lin, Z. Liu, F. Song, S. Shin, and M. Z. Hasan, Nat. Commun. **7**, 13643 (2016).

[24] Y. Xu, F. Zhang, and C. Zhang, Phys. Rev. Lett. **115**, 265304 (2015).

[25] L. Fu and C. L. Kane, Phys. Rev. Lett. **100**, 096407 (2008).

[26] J. J. He, T. K. Ng, P. A. Lee, and K. T. Law, Phys. Rev. Lett. **112**, 037001 (2014).

[27] H.-H. Sun, K.-W. Zhang, L.-H. Hu, C. Li, G.-Y. Wang, H.-Y. Ma, Z.-A. Xu, C.-L. Gao, D.-D. Guan, Y.-Y. Li, C. Liu, D. Qian, Y. Zhou, L. Fu, S.-C. Li, F.-C. Zhang, and J.-F. Jia, Phys. Rev. Lett. **116**, 257003 (2016).

[28] J. P. Xu, M. X. Wang, Z. L. Liu, J. F. Ge, X. Yang, C. Liu, Z. A. Xu, D. Guan, C. L. Gao, D. Qian, Y. Liu, Q. H. Wang, F. C. Zhang, Q. K. Xue, and J. F. Jia, Phys. Rev. Lett. **114**, 017001 (2015).

[29] B. Bradlyn, J. Cano, Z. Wang, M. G. Vergniory, C. Felser, R. J. Cava, and B. A. Bernevig, Science **353**, aaf5037 (2016).

[30] S. Zhang, L. Pi, R. Wang, G. Yu, X.-C. Pan, Z. Wei, J. Zhang, C. Xi, Z. Bai, F. Fei, M. Wang, J. Liao, Y. Li, X. Wang, F. Song, Y. Zhang, B. Wang, D. Xing, and G. Wang, arXiv:1702.03344.

[31] T. Chen, Q. Chen, K. Schouteden, W. Huang, X. Wang, Z. Li, F. Miao, X. Wang, Z. Li, B. Zhao, S. Li, F. Song, J. Wang, B. Wang, C. Van Haesendonck, and G. Wang, Nat. Commun. **5**, 5022 (2014).

[32] T. Chen, W. Liu, F. Zheng, M. Gao, X. Pan, G. van der Laan, X. Wang, Q. Zhang, F. Song, B. Wang, B. Wang, Y. Xu, G. Wang, and R. Zhang, Adv. Mater. **27**, 4823 (2015).

[33] F. Fei, Z. Wei, Q. Wang, P. Lu, S. Wang, Y. Qin, D. Pan, B. Zhao, X. Wang, J. Sun, X. Wang, P. Wang, J. Wan, J. Zhou, M. Han, F. Song, B. Wang, and G. Wang, Nano Lett. **15**, 5905 (2015).

[34] M. Udagawa and E. J. Bergholtz, Phys. Rev. Lett. **117**, 086401 (2016).

[35] T. E. O'Brien, M. Diez, and C. W. Beenakker, Phys. Rev. Lett. **116**, 236401 (2016).

[36] H. Huang, S. Zhou, and W. Duan, Phys. Rev. B **94**, 121117(R) (2016).

[37] M. Yan, H. Huang, K. Zhang, E. Wang, W. Yao, K. Deng, G. Wan, H. Zhang, M. Arita, H. Yang, Z. Sun, H. Yao, Y. Wu, S. Fan, W. Duan, and S. Zhou, arXiv:1607.03643.

[38] H.-J. Noh, J. Jeong, E.-J. Cho, K. Kim, B. I. Min, and B.-G. Park, Phys. Rev. Lett. **119**, 016401 (2017).

[39] A. E. Dunsworth, J. Low Temp. Phys. **19**, 51 (1975).

[40] v. J. Guggenheim and F. H. u. J. Müller, Helv. Phys. Acta **34**, 408 (1961).

[41] I. M. Lifshitz and A. M. Kosevich, Sov. Phys. JETP **2**, 636 (1956).

[42] J. Hu, Z. Tang, J. Liu, X. Liu, Y. Zhu, D. Graf, K. Myhro, S. Tran, C. N. Lau, J. Wei, and Z. Mao, Phys. Rev. Lett. **117**, 016602 (2016).

[43] Y. Liu, J.-Z. Zhao, L. Yu, C.-T. Lin, A.-J. Liang, C. Hu, Y. Ding, Y. Xu, S.-L. He, L. Zhao, G.-D. Liu, X.-L. Dong, J. Zhang, C.-T. Chen, Z.-Y. Xu, H.-M. Weng, X. Dai, Z. Fang, and X.-J. Zhou, Chin. Phys. Lett. **32**, 067303 (2015).

[44] A. A. Soluyanov, D. Gresch, Z. Wang, Q. Wu, M. Troyer, X. Dai, and B. A. Bernevig, Nature (London) **527**, 495 (2015).

[45] See Supplemental Material at http://link.aps.org/supplemental/10.1103/PhysRevB.96.041201 for detailed information on crystal growth and characterization, method of electronic structure calculations, and ARPES measurement at various photon energies.

[46] S.-Y. Xu, N. Alidoust, I. Belopolski, A. Richardella, C. Liu, M. Neupane, G. Bian, S.-H. Huang, R. Sankar, C. Fang, B. Dellabetta, W. Dai, Q. Li, M. J. Gilbert, F. Chou, N. Samarth, and M. Z. Hasan, Nat. Phys. **10**, 943 (2014).

[47] M.-X. Wang, C. Liu, J.-P. Xu, F. Yang, L. Miao, M.-Y. Yao, C. L. Gao, C. Shen, X. Ma, X. Chen, Zhu-An, X. Liu, S.-C. Zhang, D. Qian, J.-F. Jia, and Q.-K. Xue, Science **336**, 52 (2012).

[48] S. Yonezawa, K. Tajiri, S. Nakata, Y. Nagai, Z. Wang, K. Segawa, Y. Ando, and Y. Maeno, Nat. Phys. **13**, 123 (2017).

[49] Y. S. Hor, A. J. Williams, J. G. Checkelsky, P. Roushan, J. Seo, Q. Xu, H. W. Zandbergen, A. Yazdani, N. P. Ong, and R. J. Cava, Phys. Rev. Lett. **104**, 057001 (2010).

[50] Z. Liu, X. Yao, J. Shao, M. Zuo, L. Pi, S. Tan, C. Zhang, and Y. Zhang, J. Am. Chem. Soc. **137**, 10512 (2015).

[51] G. Bednik, A. A. Zyuzin, and A. A. Burkov, Phys. Rev. B **92**, 035153 (2015).

[52] R. Wang, L. Hao, B. Wang, and C. S. Ting, Phys. Rev. B **93**, 184511 (2016).

[53] M. Kargarian, M. Randeria, and Y. M. Lu, Proc. Natl. Acad. Sci. U.S.A. **113**, 8648 (2016).